

Surface-enhanced pair transfer in quadrupole states of neutron-rich Sn isotopes

Masayuki Matsuo, Yasuyoshi Serizawa

*Department of Physics, Faculty of Science and Graduate School of
Science and Technology, Niigata University, Niigata 950-2181, Japan*

(Dated: November 14, 2018)

We investigate the neutron pair transfer modes associated with the low-lying quadrupole states in neutron-rich Sn isotopes by means of the quasiparticle random phase approximation based on the Skyrme-Hartree-Fock-Bogoliubov mean field model. The transition strength of the quadrupole pair-addition mode feeding the 2_1^+ state is enhanced in the Sn isotopes with $A \geq 132$. The transition density of the pair-addition mode has a large spatial extension in the exterior of nucleus, reaching far to $r \sim 12 - 13$ fm. The quadrupole pair-addition mode reflects sensitively a possible increase of the effective pairing interaction strength in the surface and exterior regions of neutron-rich nuclei.

PACS numbers: 21.10.Pc, 21.10.Re, 21.60.Jz, 25.40.Hs, 27.60.+j

I. INTRODUCTION

The pair correlation is one of the fundamental nucleon many-body correlations, which governs many aspects of the nuclear structure[1–4]. Recently attentions are paid to the properties of the pair correlation in neutron-rich nuclei, which exhibit new features such as the neutron halo, the neutron skin and the presence of weakly bound neutrons. For example, a spatial two-neutron correlation or the di-neutron correlation, between two weakly-bound neutrons forming the halo in ^{11}Li and ^6He has been discussed extensively [5–10], and its experimental signatures are reported recently [11, 12]. There exists also several theoretical studies demonstrating similar spatial two-neutron correlation in many other nuclear systems. The spatial two-particle correlation was originally discussed in the closed-shell + two-particle systems [13–16], and recent selfconsistent Hartree-Fock-Bogoliubov mean-field calculations suggest that the correlation is generically enhanced around the nuclear surface of neutron-rich nuclei covering also medium- and heavy-mass regions [17–19]. Furthermore it is found that neutron matter at low densities may exhibit features of the strong coupling pairing[20–22], characterized by the small size (~ 5 fm at minimum) of the Cooper pair comparable with the average inter-neutron distance [23–25], reflecting the large scattering length $a = -18.5\text{fm}$ of the bare nuclear force. This may also suggest a possible enhancement of the pair correlation in the surface and exterior regions of neutron-rich nuclei. The spatial two-neutron correlation and the surface enhancement of the neutron pairing is also discussed in the cases of a slab and a semi-infinite nuclear matter[26, 27]. Also the pairing interaction induced by the coupling to the phonons is expected to increase the surface enhancement[28].

It is important to ask how one can probe the surface enhancement of the pair correlation in neutron-rich nuclei. We consider here the transfer of a neutron pair since the matrix element of the pair transfer has direct relation to the degree of the pair correlation[1, 2, 29–31]. Recently the neutron pair transfer process in light neutron-rich nuclei ^{11}Li and ^6He has been studied ex-

perimentally [32–35]. In the theoretical side, a possible link between the pair transfer between the 0^+ ground states and the surface enhancement of the pairing in medium and heavy neutron-rich nuclei was suggested by Dobaczewski *et al.*[36]. Recently the pair transfer feeding the excited 0^+ states in neutron-rich nuclei has been investigated [37–39] from the viewpoint of the pair vibrational mode, which are collective vibrational modes associated with the pair correlation[1, 2, 30]. Khan *et al.*[39] has argued that the pair transfer can be a possible probe of different models of the pairing interactions with differences in density dependence and surface enhancement.

In the present work, we shed light on the neutron pair transfer with the *quadrupole* multipolarity[31, 40, 41], i.e., the transitions from the ground state of a nucleus with neutron number N feeding excited 2^+ states, in particular the first 2^+ state, in the neighboring $N \pm 2$ isotopes. It is noted that the first 2^+ state in open shell nuclei is a collective state of the surface vibrational type with a strong influence by the pair correlation[1]. With this surface character of the mode, we expect that the pair transfer feeding the 2_1^+ state may provide information on the pair correlation possibly enhanced in the surface and exterior regions of neutron-rich nuclei.

The low-lying quadrupole vibration is revealed recently to show new features in some neutron-rich nuclei. For instance, the ratio between the neutron and proton amplitude becomes significantly different from the liquid drop ratio N/Z [42–47]. New aspects of the quadrupole vibration may emerge also in the pair transfer transitions feeding the 2^+ states. In our previous studies on the dipole and octupole responses, we have shown that soft modes accompanying a large pair transition amplitude in the surface and exterior regions emerge above the threshold energy in nuclei with small neutron separation energy[17, 48, 49]. We also found that these soft dipole and octupole modes are sensitive to the surface-enhancement of the pair correlation. The low-lying quadrupole vibration is different from these soft modes in many respects: it exists systematically from stable nuclei to nuclei far from the stability line, and the

excitation energy is located below the separation energy in most of the cases. Nevertheless, as we shall show below, the low-lying quadrupole mode also has sensitivity to the surface pair correlation. The sensitivity is systematically seen in the pair-addition transfer feeding the lowest-lying quadrupole state, and it becomes significant in neutron-rich nuclei beyond the shell closure, i.e. in Sn isotopes with $A \geq 132$.

We shall perform systematic numerical study by adopting the Sn isotopes as a representative case since its long isotopic chain enables us to see systematic trends. In particular we focus on isotopes beyond the $N = 82$ shell gap, above which the neutron separation energy suddenly decreases. Our study is based on the Skyrme-Hartree-Fock-Bogoliubov mean-field theory in describing the pair correlated ground state, and the quasiparticle random phase approximation (QRPA)[48] (and references in [50]) to describe the 2^+ states and the associated pair transfer modes. In the present work, we concentrate on the nuclear structure aspects, and leave the cross section and the reaction mechanism of the neutron pair transfer[31, 51–53] for future works. The formalism is described in Section 2. To elucidate effects of the surface-enhanced pairing, we compare different models of the effective pairing interaction, which have and do not have the property of the surface enhancement. After presenting the adopted effective pairing interactions in Section 3, we discuss numerical results in Section 4, and the conclusions are drawn in Section 5.

II. SKYRME-HARTREE-FOCK-BOGOLIUBOV MEAN-FIELD PLUS QRPA APPROACH

A. model

We adopt the Hartree-Fock-Bogoliubov mean-field model and the quasiparticle random phase approximation (QRPA) to describe the pair transfer modes with the quadrupole multipolarity. The basic framework of the present HFB+QRPA formalism is described in Refs.[48, 54]. Here we recapitulate it briefly in order to explain the procedure to describe the pair transfer modes.

In performing the HFB calculation, we assume the spherical symmetry for the ground state and the associated mean-fields. The Skyrme energy density functional (the energy density functional associated with the Skyrme interaction) is adopted to derive the Hartree-Fock potential and the position-dependent effective mass[55]. The parameter set SLy4 is adopted[56]. As the residual interaction responsible for the pairing correlation we use the density-dependent delta interaction (DDDI) [5, 8, 23, 36, 57–64]

$$v_q^{\text{pair}}(\mathbf{r}, \mathbf{r}') = \frac{1}{2}(1 - P_\sigma)V_q(\mathbf{r})\delta(\mathbf{r} - \mathbf{r}') \quad (q = n, p) \quad (1)$$

where the pairing interaction strength $V_q(\mathbf{r})$ is a function of the neutron and proton densities $\rho_q(\mathbf{r})$ ($q = n, p$),

and hence it depends on the position \mathbf{r} . We solve the Hartree-Fock-Bogoliubov equation in the radial coordinate space to obtain the wave functions of the quasiparticle states. We assume the box boundary condition at $r = R_{\text{max}}$ with $R_{\text{max}} = 20$ fm. We truncate the quasiparticle states by the maximum quasiparticle energy $E_{\text{max}} = 60$ MeV. We also truncate the quasiparticle states by the maximum orbital angular quantum number $l_{\text{max}} = 12$, which is sufficiently large to obtain the converged HFB solutions of the Sn isotopes.

The QRPA calculation is then performed on the basis of the self-consistent HFB mean-fields. As the residual interaction in the particle-particle channel, we adopt the DDDI, Eq. (1), the same effective pairing interaction used for the HFB calculation. Concerning the residual interaction in the particle-hole channel, we derive it also from the Skyrme functional used for the HFB calculation, but we apply the Landau-Migdal approximation to the residual interaction[37, 39, 48, 50]. Namely, we approximate the particle-hole residual interaction by a position-dependent contact interaction $v_{ph}(\mathbf{r}, \mathbf{r}') = \{(F_0/N_0)(\mathbf{r}) + (F'_0/N_0)(\mathbf{r})\boldsymbol{\tau} \cdot \boldsymbol{\tau}'\} \delta(\mathbf{r} - \mathbf{r}')$ where F_0/N_0 and F'_0/N_0 are the Landau-Migdal parameters derived from the Skyrme functional. The position dependence is taken into account in the Landau parameters by the local density approximation to the Fermi momentum. As a prescription commonly adopted in the QRPA studies using the Landau-Migdal approximation[37, 39, 48, 50], we introduce a renormalization factor f multiplying v_{ph} , and it is fixed to impose the zero excitation energy for the lowest-energy isoscalar dipole solution corresponding to the spurious center-of-mass motion.

We adopt the linear response formalism for the QRPA calculation[54]. Given the above residual interactions, we have coupled linear response equations for three kinds of fluctuating densities $\delta\rho_q(\mathbf{r}, \omega)$, $\delta\tilde{\rho}_{q,+}(\mathbf{r}, \omega)$ and $\delta\tilde{\rho}_{q,-}(\mathbf{r}, \omega)$, which correspond respectively to fluctuating parts of the nucleon density

$$\begin{aligned} \rho_q(\mathbf{r}, t) &\equiv \langle \Psi(t) | \hat{\rho}_q(\mathbf{r}) | \Psi(t) \rangle \\ &= \langle \Psi(t) | \sum_{\sigma} \psi_q^{\dagger}(\mathbf{r}\sigma)\psi_q(\mathbf{r}\sigma) | \Psi(t) \rangle \end{aligned} \quad (2)$$

and of two kinds of the pair densities

$$\tilde{\rho}_{q,\pm}(\mathbf{r}, t) \equiv \langle \Psi(t) | \psi_q^{\dagger}(\mathbf{r}\downarrow)\psi_q^{\dagger}(\mathbf{r}\uparrow) \pm \psi_q(\mathbf{r}\uparrow)\psi_q(\mathbf{r}\downarrow) | \Psi(t) \rangle. \quad (3)$$

The time-dependence of the state vector, and hence the density fluctuations $\delta\rho_q(\mathbf{r}, \omega) = Y_{LM}(\hat{\mathbf{r}})\delta\rho_q(r, \omega)/r^2$ and $\delta\tilde{\rho}_{q,\pm}(\mathbf{r}, \omega) = Y_{LM}(\hat{\mathbf{r}})\delta\tilde{\rho}_{q,\pm}(r, \omega)/r^2$ in the frequency domain arise from a response of the system caused by external fields with multipolarity L . It is convenient to introduce operators

$$P_q^{\dagger}(\mathbf{r}) = \frac{1}{2} \sum_{\sigma} \psi_q^{\dagger}(\mathbf{r}\sigma)\psi_q^{\dagger}(\mathbf{r}\tilde{\sigma}), \quad (4)$$

$$P_q(\mathbf{r}) = \frac{1}{2} \sum_{\sigma} \psi_q(\mathbf{r}\tilde{\sigma})\psi_q(\mathbf{r}\sigma). \quad (5)$$

Here $P_q^\dagger(\mathbf{r})$ and $P_q(\mathbf{r})$ represent respectively addition and removal at position \mathbf{r} of a pair of like-nucleons whose spins are coupled to the singlet $S = 0$. The pair densities are written compactly as $\tilde{\rho}_{q,\pm}(\mathbf{r}, t) = \langle \Psi(t) | P_q^\dagger(\mathbf{r}) \pm$

$P_q(\mathbf{r}) | \Psi(t) \rangle$.

For a response with the multipolarity L and the natural parity $\pi = (-)^L$, the coupled linear response equation is written in the radial coordinate system as

$$\begin{pmatrix} \delta\rho_{qL}(r, \omega) \\ \delta\tilde{\rho}_{+,qL}(r, \omega) \\ \delta\tilde{\rho}_{-,qL}(r, \omega) \end{pmatrix} = \int_0^{R_{\max}} dr' \begin{pmatrix} R_{0,qL}^{\alpha\beta}(r, r', \omega) \end{pmatrix} \begin{pmatrix} \sum_{q'} \kappa_{ph}^{qq'}(r') \delta\rho_{q'L}(r', \omega)/r'^2 + v_{0,qL}^{\text{ext}}(r') \\ \kappa_{\text{pair}}(r') \delta\tilde{\rho}_{+,qL}(r', \omega)/r'^2 + \tilde{v}_{+,qL}^{\text{ext}}(r') \\ -\kappa_{\text{pair}}(r') \delta\tilde{\rho}_{-,qL}(r', \omega)/r'^2 + \tilde{v}_{-,qL}^{\text{ext}}(r') \end{pmatrix}, \quad (6)$$

where $R_{0,qL}^{\alpha\beta}$ is the unperturbed response function representing non-interacting two-quasiparticle excitations. $\kappa_{ph}(r)$ and $\kappa_{\text{pair}}(r)$ are the residual interactions in the particle-hole and the particle-particle channels, respectively.

In the present studies we consider external fields of the pair addition and removal types

$$V_{\text{pair}}^{\text{ext}} = \int d\mathbf{r} \tilde{v}_{+,qL}^{\text{ext}}(r) Y_{LM}(\hat{\mathbf{r}}) (P_q^\dagger(\mathbf{r}) + P_q(\mathbf{r})) + \int d\mathbf{r} \tilde{v}_{-,qL}^{\text{ext}}(r) Y_{LM}(\hat{\mathbf{r}}) (P_q^\dagger(\mathbf{r}) - P_q(\mathbf{r})) \quad (7)$$

in addition to the usual external field of the particle-hole

type

$$V_{ph}^{\text{ext}} = \int d\mathbf{r} \sum_q v_{0,qL}^{\text{ext}}(r) Y_{LM}(\hat{\mathbf{r}}) \hat{\rho}_q(\mathbf{r}). \quad (8)$$

Note that the linear response equation (6) formulated in the present work contains $\tilde{v}_{\pm,qL}^{\text{ext}}(r)$ representing the pair-addition/removal fields.

For the unperturbed response function $R_{0,qL}^{\alpha\beta}$ appearing in the linear response equation (6), we adopt the spectral representation

$$R_{0,qL}^{\alpha\beta}(r, r', \omega) = \frac{1}{2} \sum_{nlj, n'l'j'} \frac{\langle l'j' || Y_L || lj \rangle^2}{2L+1} \left\{ \frac{\langle 0 | \mathcal{A} | nlj, n'l'j' \rangle_r \langle nlj, n'l'j' | \mathcal{B} | 0 \rangle_{r'}}{\hbar\omega + i\epsilon - E_{nlj} - E_{n'l'j'}} - \frac{\langle 0 | \mathcal{B} | nlj, n'l'j' \rangle_{r'} \langle nlj, n'l'j' | \mathcal{A} | 0 \rangle_r}{\hbar\omega + i\epsilon + E_{nlj} + E_{n'l'j'}} \right\}, \quad (9)$$

with

$$\begin{aligned} \langle 0 | \mathcal{A} | nlj, n'l'j' \rangle_r &\equiv \bar{\phi}_{n'l'j'}^T(r) \mathcal{A} \phi_{nlj}(r), \\ \langle nlj, n'l'j' | \mathcal{A} | 0 \rangle_r &\equiv \phi_{nlj}^T(r) \mathcal{A} \bar{\phi}_{n'l'j'}(r), \end{aligned}$$

using the discretized quasiparticle eigenstates of the HFB mean-field Hamiltonian. Here $\phi_{nlj}(r) = (\phi_{nlj}^{(1)}(r), \phi_{nlj}^{(2)}(r))^T$ is the two-component radial wave function of a quasiparticle state with the quantum number nlj , and \mathcal{A} and \mathcal{B} are 2×2 matrices defined for the three kinds of density ρ_q and $\tilde{\rho}_{q,\pm}$, Eqs.(2) and (3) (see Ref.[54], for details). ϵ is a smearing parameter, for which in the present work we adopt $\epsilon = 0.05$ MeV corresponding to a convolution of the strength function with the Lorentzian function of FWHM=100 keV. In the previous works[17, 48, 49, 54] we used the formalism which implements the continuum quasiparticle states satisfying the proper boundary conditions connecting to outgoing waves. The continuum QRPA calculation based on this formalism is useful for the states above the particle threshold energy, but, on the other hand, it costs

quite severely a large computation time, especially when we choose a small value for the smearing parameter ϵ , and it is too demanding for systematic studies. The calculated lowest 2^+ mode obtained in the present study are all located below the neutron separation energy, and we use a large box size $R_{\max} = 20$ fm. In the present study, therefore, we adopt the spectrum representation using the discretized quasiparticle states obtained in the HFB calculation. An argumentation on this point will be given later.

B. Strength function and transition density for pair transfer modes

The HFB+QRPA model enables us to calculate the transition matrix elements for pair transfer operators. Here by the pair transfer operator we mean a generalized one-body operator which either add or remove a pair of singlet neutrons. We consider the following pair-addition

operator with multipolarity L ,

$$\begin{aligned} P_{LM}^\dagger &= \int d\mathbf{r} Y_{LM}(\hat{r}) f(r) P^\dagger(\mathbf{r}) \\ &= \int d\mathbf{r} Y_{LM}(\hat{r}) f(r) \psi^\dagger(\mathbf{r} \downarrow) \psi^\dagger(\mathbf{r} \uparrow), \end{aligned} \quad (10)$$

which is essentially the same as the multipole pair operators used in the traditional works[30, 31, 40, 41]. Here and hereafter we omit the isospin index q for simplicity since we discuss only the neutron pair transfer and the neutron pairing in the present paper. Note that $f(r)$ is a form factor of the pair-addition operator, and we choose $f(r) = 1$ in the present analysis. This is a simplification, but even this simple choice is useful for discussions on isotopic trends and roles of the surface enhanced pair interactions as we show below.

The strength function for the multipole pair-addition operator P_{LM}^\dagger is given by

$$S_{\text{Pad}L}(E) \equiv \sum_{iM} \delta(E - E_{iL}) |\langle \Psi_{iLM} | P_{LM}^\dagger | \Psi_0 \rangle|^2, \quad (11)$$

where Ψ_0 and Ψ_{iLM} are the ground and the excited states obtained in the QRPA, and E_{iL} is the QRPA excitation energy. In the linear response formalism of QRPA, this quantity can be calculated as

$$S_{\text{Pad}L}(\hbar\omega) = -\frac{2L+1}{\pi} \text{Im} \int dr \frac{1}{2} (\delta\tilde{\rho}_{+,qL}(r, \omega) - \delta\tilde{\rho}_{-,qL}(r, \omega)) \quad (12)$$

using the solutions of Eq.(6) obtained with the external field

$$\mathcal{V}^{\text{ext}}(r) \equiv \begin{pmatrix} v_{0,qL}^{\text{ext}}(r) \\ \tilde{v}_{+,qL}^{\text{ext}}(r) \\ \tilde{v}_{-,qL}^{\text{ext}}(r) \end{pmatrix} = \begin{pmatrix} 0 \\ \frac{1}{2} \\ \frac{1}{2} \end{pmatrix}, \quad (13)$$

which corresponds to an external field identified to the pair-addition operator, i.e., $V_{\text{pair}}^{\text{ext}} = P_{L0}^\dagger$. We evaluate the strength

$$\begin{aligned} B(\text{Pad}L) &= \sum_M |\langle \Psi_{iLM} | P_{LM}^\dagger | \Psi_0 \rangle|^2 \\ &= (2L+1) |\langle \Psi_{iL0} | P_{L0}^\dagger | \Psi_0 \rangle|^2 \end{aligned} \quad (14)$$

associated with an individual QRPA solution by integrating the strength function $S_{\text{Pad}L}(E)$ in an energy interval $E \in [E_i - 10\epsilon, E_i + 10\epsilon]$, where E_i is the peak energy of a peak in $S_{\text{Pad}L}(E)$, corresponding to a QRPA solution, and ϵ is the smearing parameter. An isolated discrete peak has the FWHM of $2\epsilon = 100$ keV.

Similarly, we can consider the multipole pair-removal operator

$$P_{LM} = \int d\mathbf{r} Y_{LM}^*(\hat{r}) f(r) \psi_q(\mathbf{r} \uparrow) \psi_q(\mathbf{r} \downarrow) = (P_{LM}^\dagger)^\dagger, \quad (15)$$

the associated strength function

$$S_{\text{Prm}L}(E) \equiv \sum_{iM} \delta(E - E_{iL}) |\langle \Psi_{iL-M} | P_{LM} | \Psi_0 \rangle|^2, \quad (16)$$

and the strength of the pair-removal operator for the individual QRPA solution

$$\begin{aligned} B(\text{Prm}L) &= \sum_M |\langle \Psi_{iL-M} | P_{LM} | \Psi_0 \rangle|^2 \\ &= (2L+1) |\langle \Psi_{iL0} | P_{L0} | \Psi_0 \rangle|^2. \end{aligned} \quad (17)$$

The former is calculated as

$$S_{\text{Prm}L}(\hbar\omega) = -\frac{2L+1}{\pi} \text{Im} \int dr \frac{1}{2} (\delta\tilde{\rho}_{+,qL}(r, \omega) + \delta\tilde{\rho}_{-,qL}(r, \omega)) \quad (18)$$

under the external field of the multipole pair-removal operator P_{L0} :

$$\mathcal{V}^{\text{ext}}(r) = \begin{pmatrix} 0 \\ \frac{1}{2} \\ -\frac{1}{2} \end{pmatrix}. \quad (19)$$

When we calculate the strength $B(QL) = (2L+1) |\langle \Psi_{iL0} | Q_{L0} | \Psi_0 \rangle|^2$ for the multipole operator of the particle-hole type $Q_{LM} = \int d\mathbf{r} Y_{LM}(\hat{r}) r^L \hat{\rho}_q(\mathbf{r})$, we choose the external field as $\mathcal{V}^{\text{ext}}(r) = (r^L, 0, 0)^T$.

We also calculate the transition density associated with the pair-addition $\Psi_0 \xrightarrow{P^\dagger} \Psi_{iLM}$ and pair-removal transfer $\Psi_0 \xrightarrow{P} \Psi_{iL-M}$. The transition density associated with the addition/removal of a neutron singlet pair at the position \mathbf{r} is defined and factorized as

$$\begin{aligned} P_{iLM}^{(\text{ad})}(\mathbf{r}) &\equiv \langle \Psi_{iLM} | \psi^\dagger(\mathbf{r} \downarrow) \psi^\dagger(\mathbf{r} \uparrow) | \Psi_0 \rangle \\ &= \langle \Psi_{iLM} | P^\dagger(\mathbf{r}) | \Psi_0 \rangle = Y_{LM}^*(\hat{\mathbf{r}}) P_{iL}^{(\text{ad})}(r) \quad (20) \\ P_{iLM}^{(\text{rm})}(\mathbf{r}) &\equiv \langle \Psi_{iLM} | \psi(\mathbf{r} \uparrow) \psi(\mathbf{r} \downarrow) | \Psi_0 \rangle \\ &= \langle \Psi_{iLM} | P(\mathbf{r}) | \Psi_0 \rangle = Y_{LM}^*(\hat{\mathbf{r}}) P_{iL}^{(\text{rm})}(r). \quad (21) \end{aligned}$$

Here the radial transition densities are expressed using the solution of the linear response equation as

$$P_{iL}^{(\text{ad})}(r) = \frac{C}{2\pi r^2} \text{Im}(\delta\tilde{\rho}_{+,qL}(r, \omega_i) - \delta\tilde{\rho}_{-,qL}(r, \omega_i)) \quad (22)$$

$$P_{iL}^{(\text{rm})}(r) = \frac{C}{2\pi r^2} \text{Im}(\delta\tilde{\rho}_{+,qL}(r, \omega_i) + \delta\tilde{\rho}_{-,qL}(r, \omega_i)) \quad (23)$$

where $E_i = \hbar\omega_i$ is the excitation energy of the QRPA solution, and C is a normalization constant. Note that the conventional transition density of the particle-hole type is given by

$$\begin{aligned} \rho_{iq}^{ph}(\mathbf{r}) &\equiv \langle \Psi_{iLM} | \sum_{\sigma} \psi_q^\dagger(\mathbf{r}\sigma) \psi_q(\mathbf{r}\sigma) | \Psi_0 \rangle \\ &= Y_{LM}^*(\hat{\mathbf{r}}) \rho_{iqL}^{ph}(r), \end{aligned} \quad (24)$$

$$\rho_{iqL}^{ph}(r) = -\frac{C}{\pi r^2} \text{Im} \delta\rho_{qL}(r, \omega_i). \quad (25)$$

The normalization factor C is fixed so that it is consistent with the strengths $B(QL)$ or $B(\text{Pad}L)$ of the QRPA solution under consideration.

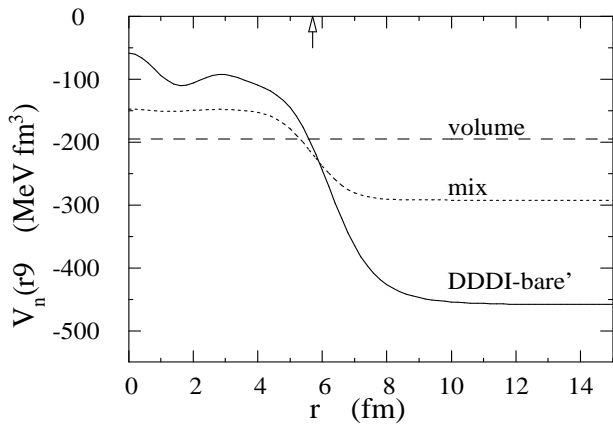


FIG. 1: The pairing interaction strength $V_n(r)$ for neutrons in ^{134}Sn , plotted as a function of the radial coordinate r for the DDDI-bare', the mix and the volume pairing interactions. The position of the half density radius is marked with the arrow.

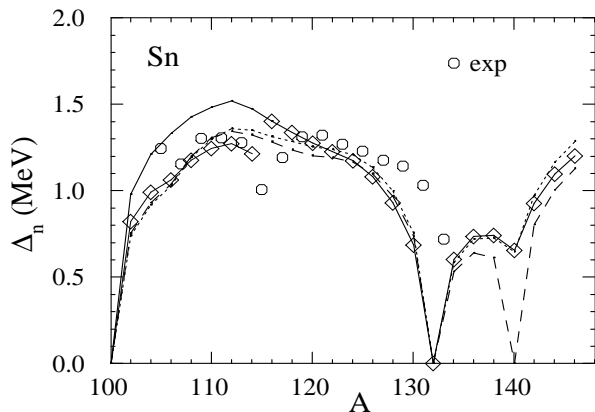


FIG. 2: The average neutron pairing gap Δ_n in the Sn isotopes. The one calculated with the DDDI-bare' ($\eta = 0.71$) is plotted with the solid line. For $100 \leq A \leq 114$, results obtained with the DDDI-bare' but using $\eta = 0.75$ is also plotted with the thin solid line and the diamond symbols. The ones calculated with the mix pairing and the volume pairing are plotted with the dotted and the dashed lines, respectively. The experimental neutron gap estimated using the three-point formula of the odd-even mass difference[65] and the mass compilation[66] is also plotted with the circles.

III. EFFECTIVE PAIRING INTERACTIONS

In the present paper we intend to disclose influences of the surface enhanced pairing on the low-lying quadrupole vibrational mode. For this purpose, we compare three versions of DDDI, Eq.(6), which have different properties concerning the surface enhancement. They are 1) the density-dependent pairing interaction which has a connection to the bare nuclear force via the scattering length, 2) the density-independent delta interaction, and 3) the so-called mix pairing interaction[60–62].

1) The first is the one which we adopt mainly in the following analysis, and it is a version of DDDI which

reproduces properties of the bare nuclear force relevant for the pairing, in particular, the scattering length of the bare force[5, 23, 24, 57, 58]. Among such DDDI's, we adopt the parametrization

$$V_n(\mathbf{r}) = v_0 \left(1 - \eta \left(\frac{\rho_n(\mathbf{r})}{\rho_c} \right)^\alpha \right) \quad (26)$$

for the interaction of neutrons[23, 49]. Here the parameter v_0 is chosen to reproduce the scattering length $a = -18.5\text{fm}$ in the 1S channel. The density-dependence characterized by the power α and the prefactor η is adjusted to reproduce the neutron pairing gap in dilute and uniform matter, more specifically the pairing gap obtained with the bare force and the BCS approximation. We find a parameter set $v_0 = -458.4 \text{ MeV fm}^{-3}$, $\rho_c = 0.08\text{fm}^{-3}$, $\alpha = 0.845$, and $\eta = 0.845$ for the quasi-particle energy cut-off with $E_{cut} = 60\text{MeV}$ [23]. However this parameter set leads to neutron pairing gaps in Sn isotopes which are systematically smaller than the empirical values estimated from the odd-even mass difference using the three-point formula[65]. We therefore vary η and fix to $\eta = 0.71$ so as to reproduce the empirical gap in ^{120}Sn [49] while keeping the scattering length relevant to the low-density limit. We call this parameter set DDDI-bare' since it is referred to the bare nucleon force, but with a small modification.

2) The second is the simplest density-independent delta interaction:

$$V_n(\mathbf{r}) = v_0. \quad (27)$$

The only relevant parameter v_0 is fixed to $v_0 = -195 \text{ MeVfm}^3$ to reproduce the gap in ^{120}Sn , as is done in Ref.[60, 62]. The density-independent delta interaction is often called the volume pairing interaction[36].

3) The third is the so-called mix pairing interaction[61, 62], which has a linear dependence on the total nucleon density $\rho(r)$, and given by

$$V_n(\mathbf{r}) = v_0 \left(1 - \frac{1}{2} \left(\frac{\rho(\mathbf{r})}{\rho_0} \right) \right) \quad (28)$$

with $\rho_0 = 0.16\text{fm}^{-3}$. Here the parameter v_0 is fixed to reproduce the gap in ^{120}Sn , leading to $v_0 = -292 \text{ MeVfm}^3$.

The pairing force strength $V_n(\mathbf{r})$ is compared among the three kinds of interaction in Fig.1, which plots $V_n(r)$ as a function of the radial coordinate in ^{134}Sn . It is seen that the DDDI-bare' exhibits the strongest radial dependence, i.e., the strongest density dependence, and that the interaction strength in the region outer than the nuclear surface (corresponding to the low density limit $\rho(r) \rightarrow 0$) is more than twice larger than that of the volume pairing. The mix pairing exhibits an intermediate radial- (density-) dependence. Since these three versions of DDDI have very different force strength in the external region we expect to see the difference in physical observables related to the surface region and/or in the exterior of nuclei.

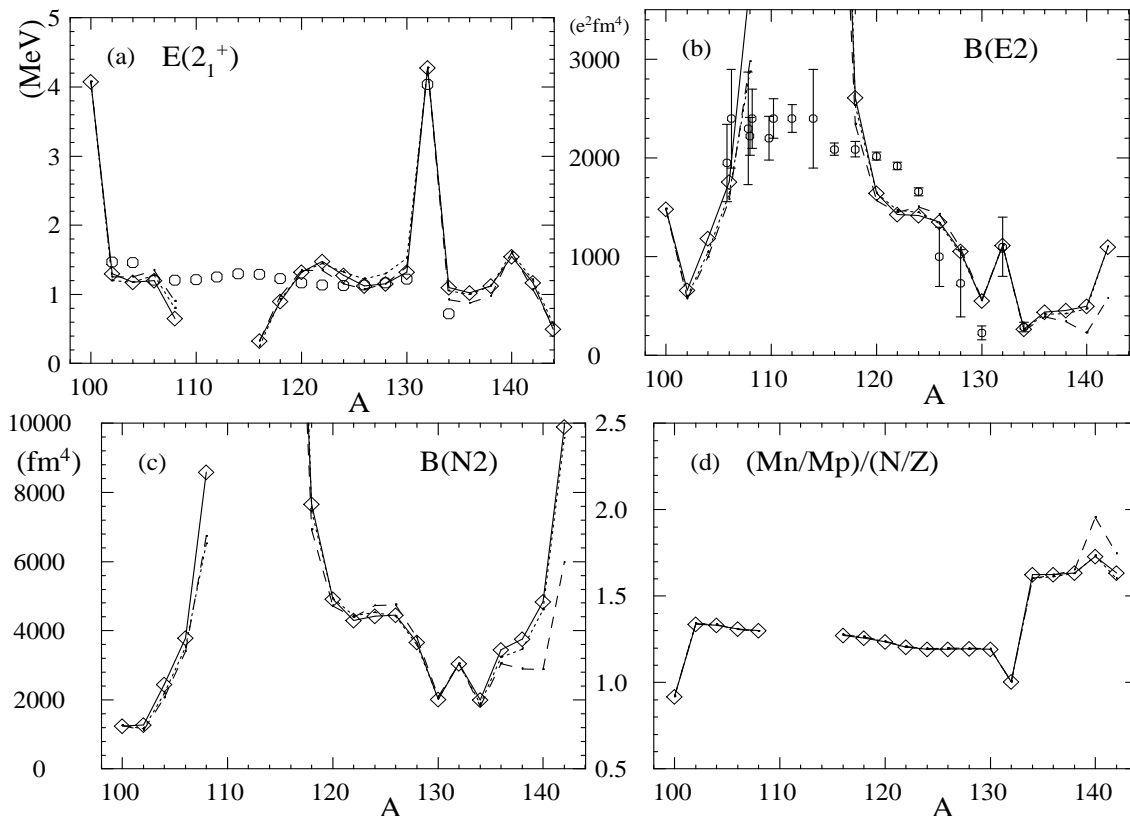


FIG. 3: (a) The excitation energy of the calculated 2_1^+ QRPA solutions obtained with the DDDI-bare', the mix and the volume pairing interactions, plotted with the diamonds connected by the solid line, the dotted line, and the dashed line, respectively. The experimental 2_1^+ energy [72] is plotted with the circles. (b) The same but for $B(E2; 0_{gs}^+ \rightarrow 2_1^+)$. The experimental data is taken from Refs. [72–77] (c) The same but for the neutron quadrupole strength $B(N2; 0_{gs}^+ \rightarrow 2_1^+)$, and (d) for the ratio $(M_n/M_p)/(N/Z)$ of the neutron and proton amplitudes associated with the 2_1^+ QRPA solution.

We compare in Fig.2 the calculated average neutron pairing gap $\Delta_n \equiv \int \Delta(\mathbf{r})_n \tilde{\rho}_n(\mathbf{r}) d\mathbf{r} / \int \tilde{\rho}_n(\mathbf{r}) d\mathbf{r}$ obtained with the three interactions. It is seen that they give the average pairing gaps which are almost identical for $A \sim 116 - 130$. In neutron-rich nuclei $A = 134 - 138$ beyond the $N = 82$ shell closure, a small difference of the order of < 150 keV is seen (except the subshell nucleus ^{140}Sn where the volume pairing gives the vanishing gap). It is pointed out in the literature [60–63] that the surface enhancement of the pairing interaction influences the average pairing gap only to a small extent unless one sees the trend in a very wide range of mass [61, 62], and the difference may grow only in very neutron-rich nuclei close to the drip-line [60, 63]. On the other hand, it is seen that the DDDI-bare' gives an overestimate of the average pairing gap for the isotopes with $A \lesssim 116$, by about $\gtrsim 200$ keV compared with the other two interactions. For a fair comparison in the following analysis, we modify slightly the value of η , i.e., $\eta = 0.75$, only for $A < 116$ so that it gives the average pairing gap comparable with those of the volume and the mixed pairing (cf. the thin solid line in Fig.2).

IV. RESULTS

In the first two subsections we will mainly discuss results which we obtain with the effective pairing interaction DDDI-bare' having the strong increase of the interaction strength in the surface and the external regions. A comparative analysis using different pairing interactions will be presented in the subsection IV C.

A. The lowest-lying quadrupole state

Let us first discuss the basic properties of the calculated lowest-lying quadrupole state, on which we focus in the present paper. Figure 3(a) and (b) shows the excitation energy $E(2_1^+)$ and $B(E2; 0_{gs}^+ \rightarrow 2_1^+)$ of the 2_1^+ QRPA solution in the Sn isotopes. The results are similar to those in the full self-consistent QRPA calculation [68] using the same Skyrme interaction SLy4. It is seen in Fig. 3(a) and (b) that the calculated $E(2_1^+)$ and $B(E2)$ reproduce reasonably well the experimental values. In the present QRPA calculation the lowest quadrupole mode shows an instability in the $A = 110 - 114$ and $A > 144$ isotopes as is also seen in Ref. [68]. We do not

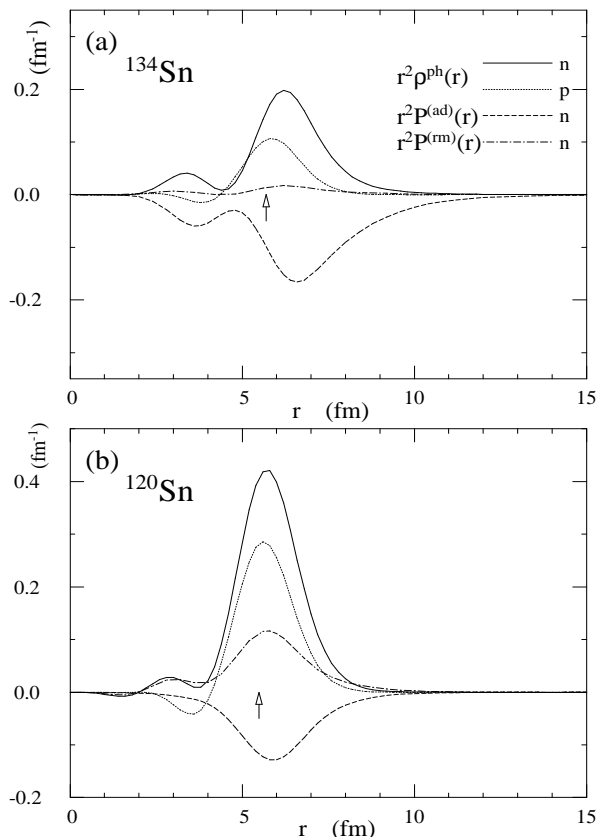


FIG. 4: The transition densities associated with the 2_1^+ QRPA solution (a) in ^{134}Sn and (b) in ^{120}Sn . The solid and the dotted curves are the particle-hole transition density $r^2\rho^{ph}(r)$ for neutrons and protons respectively while the dashed and the dot-dashed curves represent the pair-addition transition density $r^2P^{(ad)}(r)$ and the pair-removal transition density $r^2P^{(rm)}(r)$ of neutrons, respectively. The arrow indicates the half density radius $R_{1/2}$. The effective pairing interaction is the DDDI-bare’.

discuss these cases and the $A = 116, 144$ cases where the QRPA excitation energy is less than 0.5 MeV since the quadrupole mode then needs to be described as an anharmonic vibration, which is beyond the scope of the present work. Note that there exist a few other QRPA calculations for the neutron-rich Sn[69, 70].

The lowest-lying quadrupole state in isotopes beyond the $N = 82$ shell closure are of special interest. Figure 3(c) shows the neutron quadrupole strength $B(N2; 0_{gs}^+ \rightarrow 2_1^+)$ calculated in the same way as $B(E2)$, but for neutrons instead of protons. The isotopic dependences of $B(E2)$ and $B(N2)$ look similar for $N < 82$, but the values of $B(N2)$ are apparently larger than the proton strength $B(E2)/e^2$ as the neutron number exceeds the magic number $N = 82$. This behavior is seen clearly in the ratio $M_n/M_p \equiv \sqrt{B(N2)/(B(E2)/e^2)}$ of the neutron and proton amplitudes, plotted in Fig. 3(d). If the low-lying quadrupole mode is a collective surface oscillation of liquid drop of uniform mixture of neutrons and protons, the ratio M_n/M_p would be N/Z . The calculated double ra-

tio $(M_n/M_p)/(N/Z)$ is around 1.2-1.3 for $A < 132$, being not very different from the liquid drop limit 1, and it is consistent with the typical values ($\approx 1.3 - 1.5$) evaluated experimentally in stable isotopes $^{116-124}\text{Sn}$ [78]. The double ratio, however, increases suddenly in $A > 132$, and amounts to 1.6-1.7. The ratio M_n/M_p itself reaches 2.7-3.1. In the isotopes beyond $N = 82$, the amplitude M_n of neutrons dominates over that M_p of protons in the first 2^+ state. Note that the $(M_n/M_p)/(N/Z)$ ratio obtained in Ref.[70, 71] is somewhat smaller than our values by about 0.2.

A characteristic feature of the lowest-lying quadrupole states beyond the $N = 82$ shell gap can be demonstrated more explicitly in terms of the transition densities, which are shown in Fig.4 for (a) ^{134}Sn and (b) ^{120}Sn . In ^{120}Sn , the transition densities exhibit the features typical of the low-lying quadrupole surface vibration. Namely, the particle-hole transition densities for neutrons and protons, and the pair-addition and -removal transition densities of neutrons exhibit similar radial profile all of which have peaks around the nuclear surface $r \sim R_{1/2} \approx 5.5$ fm ($R_{1/2}$ denotes the half-density radius defined by $\rho(r) = 0.08$ fm $^{-3}$). In ^{134}Sn , in contrast, the peak positions of the neutron and proton particle-hole transition density $\rho_{n,p}^{ph}(r)$ deviates significantly with each other: the neutron transition density has amplitude which extends toward the exterior of the nucleus while the proton transition density does not.

The transition density $P^{(ad)}(r)$ of the neutron pair-addition mode is most characteristic in ^{134}Sn . It has the largest amplitude in the external region $r \gtrsim R_{1/2}$ (≈ 5.7 fm) among the three kinds of transition densities. The position where the amplitude of $P^{(ad)}(r)$ is maximum, $r \approx 6.6$ fm, deviates by about 1fm from the nuclear surface ($r \approx 5.7$ fm), and it is even outside of the peak position of the neutron particle-hole transition density. In addition, it is extended significantly toward the outside of the nucleus, and the tail reaches far to 12-13 fm (in the scale of the figure). The extension of the amplitude in the external region is much more significant than that in the neutron particle-hole transition density $\rho^{ph}(r)$. We note also that the transition density $P^{(rm)}(r)$ of the neutron pair-removal mode is very small in comparison with the pair-addition transition density $P^{(ad)}(r)$, and the dominance of the pair-addition amplitude is commonly seen in all the cases of $^{134-142}\text{Sn}$.

B. Quadrupole pair transfer

Figure 5 shows the strength functions $S_{\text{Pad}2}(E)$ and $S_{\text{Prm}2}(E)$ for the quadrupole pair-addition and -removal modes in ^{134}Sn and ^{120}Sn . The pair-addition strength associated with the first 2^+ mode in ^{134}Sn is significantly larger than that in ^{120}Sn , and it reflects the large pair-addition amplitude seen in Fig.4. The unperturbed strength functions are also plotted for comparison (the dotted curve). The first peak in the unperturbed cal-

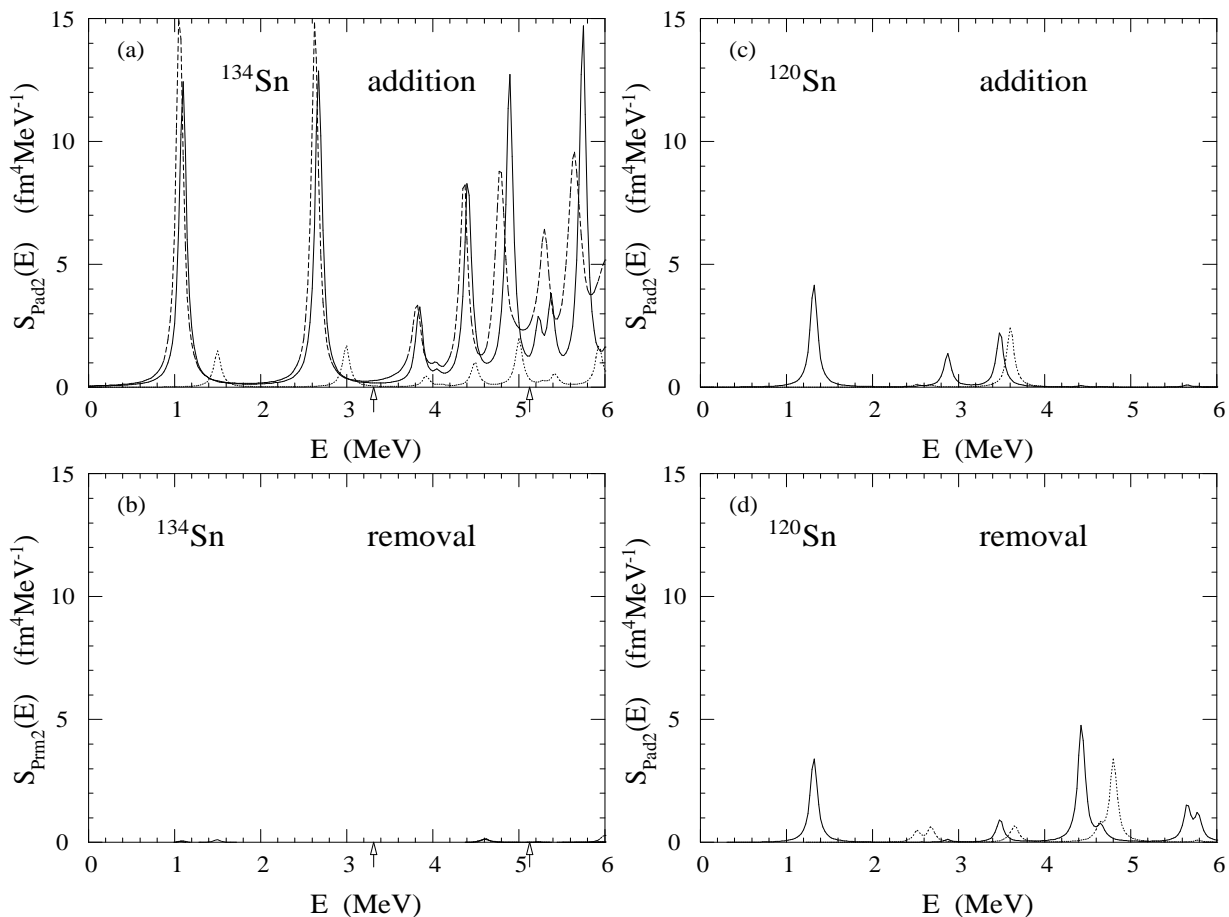


FIG. 5: (a) The transition strength function $S_{\text{Pad}2}(E)$ for the quadrupole pair-addition mode in ^{134}Sn , plotted with the solid curve. The thin dashed curve is the result of the continuum QRPA calculation while the dotted curve represents the unperturbed response for the two-quasiparticle excitations. The effective pairing interaction is the DDDI-bare'. The smearing parameter is $\epsilon = 50$ keV. The arrows indicate the calculated one- and two-neutron separation energies S_{1n} and S_{2n} . (b) The same as (a) but for the transition strength function $S_{\text{P}m2}(E)$ for the quadrupole pair-removal mode. (c)(d) The same as (a) and (b), but for ^{120}Sn .

culcation of ^{134}Sn corresponds to the transition to the two-quasi-neutron configuration $[1f_{7/2}]^2_{I=2}$. The pair-addition strength for the 2_1^+ state in the full calculation is about ten times larger than that in the unperturbed calculation, thus it indicates a significant enhancement due to a collectivity (the RPA correlation in the other words) in the pair-addition mode. Another feature observed in ^{134}Sn is that the RPA correlation effect is large not only for the lowest mode but also for higher lying modes: the second peak of $S_{\text{Pad}2}(E)$ also has a large pair-addition strength comparable with the first peak, and there exist several peaks in the excitation energy region $E \gtrsim 4$ MeV with significant pair-addition strength. The peaks above the one-neutron separation energy S_{1n} are discretized continuum states. The continuum QRPA calculation[48, 54] is appropriate for the excitation energies above S_{1n} . In fact, the result of the continuum QRPA calculation, shown with the thin dashed curve in Fig. 5, indicates that the proper treatment of the continuum modifies the strength function for $E > S_{1n}$. On the

other hand, it has only a minor effect on the strengths below S_{1n} , and it does not affect the discussions below. Note also that the pair-removal strength in ^{134}Sn is extremely small in the displayed energy range.

1. pair-addition mode

We shall discuss properties of the pair-addition mode in detail. Figure 6(a) is the systematics of the pair-addition strength $B(\text{Pad}2)$ associated with the 2_1^+ mode. A feature immediately noticed in the figure is a strong variation along the isotopic chain. $B(\text{Pad}2)$ takes a rather small value for $A < 132$, but it shows a big jump at $A = 132$, where the strength is larger than those in any other isotopes with $A < 132$. Proceeding from ^{132}Sn to ^{134}Sn , ^{136}Sn and ^{138}Sn , the strength decreases gradually while keeping relatively large values. It then turns to increase in ^{140}Sn . and takes a very large value in ^{142}Sn .

Figure 7(a) shows the pair-addition transition densities

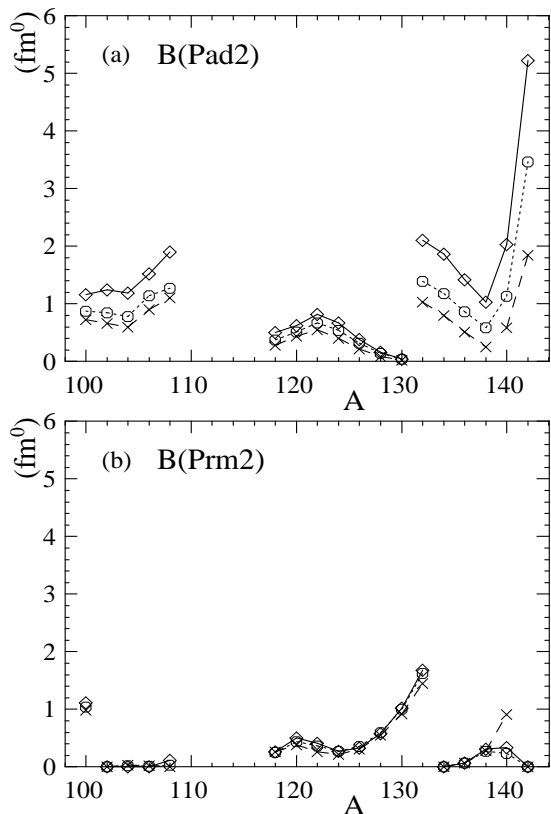


FIG. 6: (a) The calculated transition strength $B(\text{Pad}2)$ of the neutron pair-addition transfer feeding the 2_1^+ states in Sn isotopes. The diamonds connected with the solid line are the results obtained with DDDI-bare' while the dotted and the dashed lines (the circles and the crosses) are for the mix and the volume pairing interactions, respectively. (b) The same but for the strength $B(\text{Prm}2)$ of the quadrupole pair removal transfer.

$P^{(\text{ad})}(r)$ associated with the lowest quadrupole mode in the isotopes $^{132-142}\text{Sn}$ beyond the $N = 82$ shell closure. It is seen that they all exhibit sizable amplitudes extending to $r \gtrsim 8$ fm as is found in Fig.4 in the case of ^{134}Sn . The spatial extension of the pair-addition transition density develops further in ^{140}Sn and ^{142}Sn , for which we see significant amplitude even around $r \sim 12-13$ fm, which is about ~ 7 fm apart from the half density surface $R_{1/2} = 5.6 - 5.8$ fm. This is contrasted with the pair-addition transition density for the isotopes $^{120-130}\text{Sn}$ below the shell closure (displayed in Fig.7(b)). In these nuclei spatial extension is hardly seen in the pair-addition transition density, and the transition densities is mostly concentrated in the internal and surface region $r \lesssim R_{1/2} + 2$ fm ≈ 8 fm. The spatial extension emerges suddenly at $A = 132$. Comparing the pair-addition transition density in ^{122}Sn (the largest one in Fig.7(b)) with that in ^{136}Sn (the third largest one among the solid curves in Fig.7(a)), the maximum amplitude is almost the same, but the pair-addition strength $B(\text{Pad}2)$ in ^{136}Sn ($B(\text{Pad}2) = 1.42$) is about twice as large as that in ^{122}Sn ($B(\text{Pad}2) = 0.82$) because of the spatial extension in ^{136}Sn .

The sudden change across the $N = 82$ shell closure may be ascribed to the fact that the isotopes with $A > 132$ have a feature of weakly bound nuclei although they are located far from the neutron drip-line. The calculated one-neutron separation energy suddenly change from $S_{1n} = 7.62$ MeV in ^{132}Sn to $S_{1n} = 3.32$ MeV in ^{134}Sn . This arises from the shell gap at $N = 82$ and from the fact that the neutron single-particle orbits $1f_{7/2}$ and $3p_{3/2}$ lying above the $N = 82$ shell gap are bound only weakly (the Hartree-Fock single-particle energies in ^{132}Sn are $e_{1f_{7/2}} = -1.99$ MeV and $e_{3p_{3/2}} = -0.25$ MeV). These orbits have significantly small binding energies compared with the orbit $h_{11/2}$ just below the shell gap ($e_{h_{11/2}} = -7.68$ MeV). Since the quadrupole pair-addition mode in ^{132}Sn and heavier isotopes necessarily contain two-quasiparticle components consisting of these weakly bound orbits, the pair-addition transition density should inherit the long tail arising from the weak binding. In particular, approaching ^{140}Sn and ^{142}Sn , neutrons start to occupy the $3p_{3/2}$ orbit which has a very small binding energy.

We remark that the closing of shells has a strong influence on the pair transfer in general[31]. For instance, the neutron shell is closed at $A = 132$ ($N = 82$) and the calculated neutron pairing gap vanishes there. In this case, the QRPA equation (6) is decomposed into the particle-hole, the particle-particle, and the hole-hole sectors. The pair-addition mode in ^{132}Sn belongs to the particle-particle sector, and the lowest-lying QRPA solution in this sector has a character of a correlated pair of neutrons built upon the ^{132}Sn core. It is nothing but the quadrupole pair vibrational mode in closed shell nuclei, and in this case a large collectivity in the pair-addition mode is known, with a typical example of ^{208}Pb [31, 40, 41]. This is, however, only one of the mechanisms of the large pair-addition strength $B(\text{Pad}2)$ seen at $A = 132$ ($N = 82$). We note that the strength in ^{132}Sn for the DDDI-bare' interaction is more than twice larger than that in ^{100}Sn (another shell closure at $N = 50$), and this relative enhancement at ^{132}Sn is a consequence of the characteristic spatial extension of the transition density in the isotopes beyond the $N = 82$ shell closure.

2. pair-removal mode

Figure 6 (b) shows the systematics of the pair-removal strength $B(\text{Prm}2)$ for transition from the ground state of an isotope A to the 2_1^+ state in the isotope $A - 2$. It is seen that the pair-removal strength is generally small, compared with the pair-addition strength. Another trend seen here is that the pair-removal strength is very small at the beginning of shells (at $A \approx 102, 134$) and of a subshell (at $A = 142$); it takes a value comparable with the pair-addition strength $B(\text{Pad}2)$ around the mid-shell ($A \sim 120$), and it is relatively large at $A = 100, 132$ because of the shell closures at $N = 50$ and $N = 82$ in parallel to the situation in ^{208}Pb . [31]

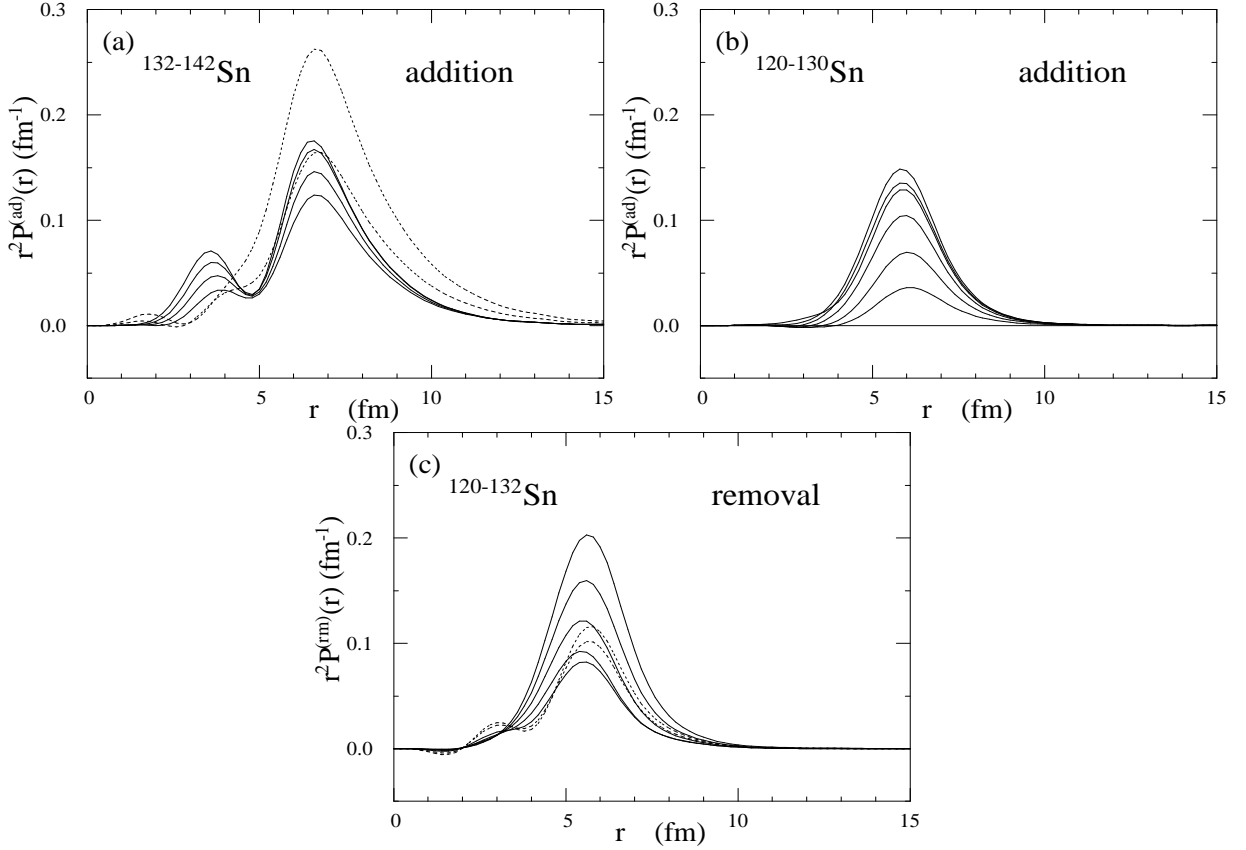


FIG. 7: (a) The transition density $r^2 P^{(\text{ad})}(r)$ for the neutron pair-addition transfer associated with the 2_1^+ QRPA solutions, calculated in the isotopes $^{132-142}\text{Sn}$. The pair-addition transition strength $B(\text{Pad}2)$ is used to normalize, and the phase is chosen so that the transition matrix element becomes positive. The solid curve is for $^{120-132}\text{Sn}$ while the dotted curve is used for $^{140-142}\text{Sn}$. The effective pairing interaction is the DDDI-bare'. (b) The same as (a), but for $^{120-130}\text{Sn}$. (c) The transition density $r^2 P^{(\text{rm})}(r)$ for the neutron pair-removal transfer associated with the 2_1^+ QRPA solutions, calculated in $^{120-132}\text{Sn}$. The solid and the dotted curves are for $^{124-132}\text{Sn}$ and $^{120,122}\text{Sn}$, respectively.

Figure 7(c) displays the pair-removal transition densities $P^{(\text{rm})}(r)$ associated with the 2_1^+ mode in the isotopes from ^{120}Sn (located in the middle of the shell) to ^{132}Sn (at the end of the shell). It is seen that the transition densities $P^{(\text{rm})}(r)$ of the pair-removal mode in these isotopes does not exhibit the spatial extension toward the outside, rather it is concentrated only around and inside the surface region $r \lesssim R_{1/2} + 2 \text{ fm} \sim 8 \text{ fm}$. This feature originates from the fact that the pair-removal transition consists mainly of the orbits situated near the Fermi energy and those bound more deeply. In the isotopes with $A \leq 132$, these are strongly bound orbits with the binding energy $e_{s.p.} \lesssim -7 \text{ MeV}$ (e.g., $e_{h_{11/2}} = -7.68 \text{ MeV}$ in ^{132}Sn) and they do not have tails extending far outside the nuclear surface.

C. Sensitivity to the surface-enhanced pairing

We shall now discuss the role of the residual pairing interaction and the sensitivity of the quadrupole pair transfer to the enhancement of the pairing interaction

in the surface and the external regions of a nucleus. In Fig.8 we compare the pair-addition strength function in ^{134}Sn and ^{120}Sn , calculated with two pairing interactions, the DDDI-bare' and the volume pairing, which have very different density-dependence in the pairing interaction strength (cf. Fig.1). In the case of ^{134}Sn we see a large difference in the quadrupole pair-addition strength in ^{134}Sn while in the case of ^{120}Sn the difference is small.

A systematic comparison is made in Fig.6 for the pair-addition and -removal strengths $B(\text{Pad}2)$ and $B(\text{Prm}2)$ of the 2_1^+ mode calculated with the three kinds of the pairing interactions, including the mix pairing as well. It is seen that the pair-addition strength exhibits a sensitivity in all the nuclei to some extent, and the sensitivity becomes prominent in $^{132-142}\text{Sn}$. The ratio of $B(\text{Pad}2)$ obtained with the DDDI-bare' and that with the volume pairing is 2.3, 2.8, 4.0, 3.5, 2.8 for $A = 134, 136, 138, 140, 142$, respectively, while for $A < 132$ it is in the range 1.4-2.0. Note, on the other hand, that the pair-removal strength $B(\text{Prm}2)$ is much less sensitive in all the isotopes. The difference in $B(\text{Prm}2)$ for the different pairing interactions is negligible in many isotopes.

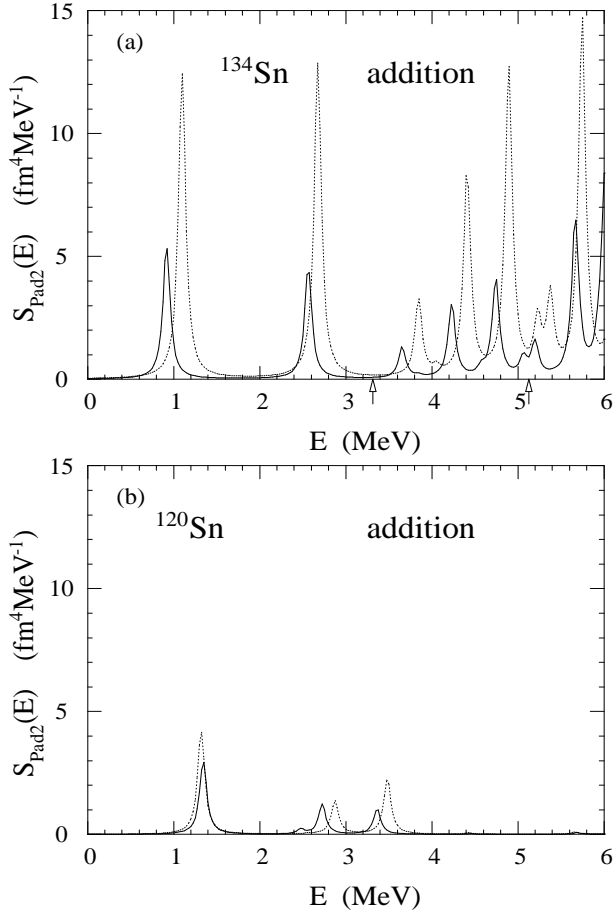


FIG. 8: Comparison of the transition strength functions $S_{\text{Pad}2}(E)$ for the neutron quadrupole pair-addition transfer, calculated with the volume pairing interaction (solid curve) and with the DDDI-bare' (dotted curve). (a) and (b) are for ^{134}Sn and ^{120}Sn , respectively.

Let us analyze the mechanism of the sensitivity of the pair-addition strength by looking into the transition densities. We show in Fig. 9 (a)-(c) the transition density $P^{(\text{ad})}(r)$ of the pair-addition mode calculated with different pairing interactions in the three representative Sn isotopes. In this figure we see an intimate relation between the degree of sensitivity and the radial profile of the transition density. Namely a large sensitivity observed in ^{134}Sn and ^{142}Sn can be linked to the pair-addition transition density extending far outside the nuclear surface, $r \gtrsim R_{1/2} + 2\text{fm}$. The sensitivity is small in ^{120}Sn where the transition density is confined mostly within the surface region $r \lesssim R_{1/2} + 2\text{fm}$.

For more detailed discussion let us examine the values of the pair-addition transition density $P^{(\text{ad})}(r)$ in ^{134}Sn at $r = 5.8, 7.8, 9.8\text{ fm}$, corresponding approximately to the half density radius $r = R_{1/2}$ ($= 5.70\text{ fm}$), and $r = R_{1/2} + 2\text{ fm}$, and $r = R_{1/2} + 4\text{ fm}$. The ratio of $P^{(\text{ad})}(r)$ obtained with the DDDI-bare' and that with the volume pairing is 1.45, 1.82 and 2.71 for $r = 5.8, 7.8, 9.8\text{ fm}$, respectively, indicating an increase of the sensitivity as

moving from the surface toward the outside.

It is also useful to compare $P^{(\text{ad})}(r)$ with the transition density $P_{\text{unp}}^{(\text{ad})}(r)$ associated with the unperturbed pair-addition transfer (i.e. the transition associated with the lowest-energy two-quasiparticle excitation obtained by neglecting the residual pairing interaction), which is also shown in Fig.9 with the dotted curve. The ratio between the transition density $P^{(\text{ad})}(r)$ obtained with the DDDI-bare' (or the volume pairing) and the unperturbed transition density $P_{\text{unp}}^{(\text{ad})}(r)$ is a measure of the influence of the RPA correlation (the configuration mixing) caused by the residual pairing interaction. In the case of the DDDI-bare', the ratio $P^{(\text{ad})}(r)/P_{\text{unp}}^{(\text{ad})}(r)$ reads 2.7 at the nuclear surface $r = R_{1/2}$, and it increases to 3.8-6.2 at $r = (R_{1/2} + 2\text{fm}) - (R_{1/2} + 4\text{fm}) \approx 8 - 10\text{fm}$. This is in contrast to the volume pairing causing much smaller ratio 1.9-2.1-2.3 at the same positions. We see even stronger sensitivity to the density-dependence of the pair interaction in ^{142}Sn , for which the tail extends further outside.

We thus see that the strong sensitivity of the pair-addition transfer originates from the RPA correlation taking place in the surface and exterior regions in ^{134}Sn and ^{142}Sn . We recall the reader here that the three pairing interactions have interaction strengths different by a factor of more than 2 (cf. Fig.1) at the positions $r \gtrsim R_{1/2} + 2\text{ fm}$ corresponding to low densities $\rho/\rho_0 \lesssim 0.1$.

A contrasting case is ^{120}Sn shown in Fig. 9(c), in which we see very little the RPA correlation effect and the difference between the DDDI-bare' and the volume pairing interactions. This is what we can expect from the discussions above as there is essentially no significant spatial extension of the pair-addition transition density in this tightly bound stable isotope, as seen in Fig. 9(c).

In Fig. 9(d) we show the transition density $P^{(\text{rm})}(r)$ of the pair-removal mode in ^{132}Sn . In this case the pair-removal amplitude is concentrated only in the vicinity and the inside of the surface $r \lesssim R_{1/2} + 2\text{ fm}$, exhibiting a very different radial profile from that of the pair-addition mode in $^{134,142}\text{Sn}$ (Fig. 9(a) and (b)). It is also seen that the pair-removal transition density $P^{(\text{rm})}(r)$ does not depend on which we adopt the DDDI-bare' or the volume pairing. We can interpret this insensitivity in terms of Fig. 1: the effective pairing strengths of the three interactions are comparable in size on average in the region $|r - R_{1/2}| \lesssim 2\text{ fm}$ where the transition strength is concentrated.

Finally we remark that the three pairing interactions give essentially identical results for $E(2_1^+)$ and $B(E2)$ except for $A \geq 140$, as is seen in Fig. 3 (a) and (b). The excitation energy and the $B(E2)$ of the 2_1^+ state in superfluid nuclei is known to depend on the pairing correlation[1]. However, the results indicate that these quantities are not influenced very much by the density-dependence of the pairing interaction as far as the average pairing gap is constrained to the same value.

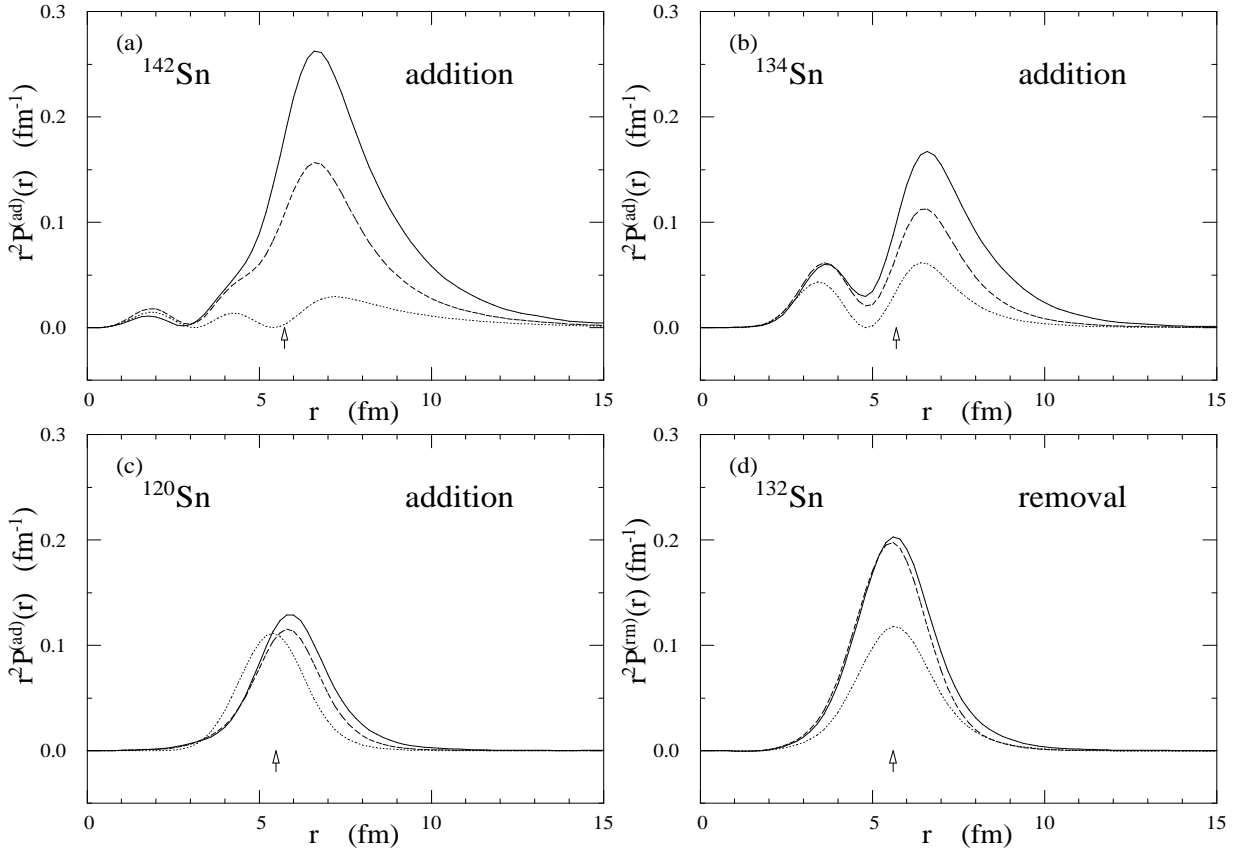


FIG. 9: Effects of the pairing residual interactions on the neutron pair-addition transition density $r^2 P^{(\text{ad})}(r)$ feeding the 2_1^+ states, calculated for the isotopes (a) ^{142}Sn , (b) ^{134}Sn , and (c) ^{120}Sn . The solid and the dashed curves are the results obtained with the DDDI-bare' and the volume pairing, respectively, while the unperturbed pair-addition transition density $r^2 P_{\text{unp}}^{(\text{ad})}(r)$ neglecting the residual interaction is also plotted with the dotted curve. The arrow indicates the position of the half density radius $R_{1/2}$. (d) The same as (a-c), but for the pair-removal transition density $r^2 P^{(\text{rm})}(r)$ of the 2_1^+ pair-removal mode in ^{132}Sn .

V. CONCLUSIONS

We have investigated the neutron pair transfer modes with the quadrupole multipolarity feeding the low-lying quadrupole states in the neutron-rich Sn isotopes by means of the QRPA based on the Skyrme-Hartree-Fock-Bogoliubov mean-fields. As a model of the surface-enhanced pairing, we used the density-dependent delta interaction (DDDI) whose strength increases at low nucleon densities reflecting the large scattering length of the 1S bare interaction in the free space.

The numerical calculations indicate that the lowest-lying quadrupole state exhibits a sudden change of its character as the neutron number increases across the magic number $N = 82$, beyond which features of weakly binding emerge in the neutron motion. The most noticeable feature is found in the pair-addition mode. Namely the transition density of the pair-addition mode feeding the 2_1^+ state extends spatially far outside the nuclear surface with a long tail reaching $r \sim 12 - 13$ fm in the isotopes $^{>132}\text{Sn}$. Accordingly the strength of the quadrupole neutron pair-addition transition is enhanced for $A > 132$. The enhanced pair-addition transfer is a

consequence of the RPA correlation caused by the pairing interaction acting strongly in the surface and external regions of a nucleus.

Comparing with other DDDI's having different density dependence, i.e. the density-independent volume pairing and the mixed pairing having an intermediate density dependence, it is found that the quadrupole pair-addition mode exhibits generally sensitivity to the increase of the pairing interaction strength in the surface and the external regions of a nucleus. The sensitivity of the pair-addition mode to the three interactions is about a factor of 1.4-2.0 in the isotopes with $A < 132$, and it is magnified to a factor of 2.0-4.0 in the isotopes $A > 132$. Therefore one can expect that the neutron pair-addition transfer feeding the 2_1^+ state in the neighboring $A + 2$ isotope, especially those feeding the isotopes $A > 132$, provides a probe to the enhancement of the pairing interaction strength expected in the surface and the external regions. On the other hand, the neutron pair-removal transfer feeding the 2_1^+ state in the $A - 2$ isotope does not have the sensitivity, and neither $B(E2)$ nor the quadrupole neutron strength $B(N2)$ does, as far as the Sn isotopes analyzed in the present work are concerned.

Acknowledgments

One of the authors (M.M.) thanks Prof. M. Kawai, Prof. M. Ichimura and Prof. A. Vitturi for useful discussions. A part of the numerical calculations were performed on the NEC SX-8 supercomputer systems at Yukawa Institute for Theoretical Physics, Kyoto Univer-

sity, and at Research Center for Nuclear Physics, Osaka University. The work was supported by the Grant-in-Aid for Scientific Research (Nos. 20540259, 21105507 and 21340073) from the Japan Society for the Promotion of Science, and also by the JSPS Core-to-Core Program, International Research Network for Exotic Femto Systems(EFES).

-
- [1] A. Bohr and B. R. Mottelson, *Nuclear Structure* vol. II (Benjamin, 1975).
- [2] D. M. Brink and R. A. Broglia, *Nuclear Superfluidity: Pairing in Finite Systems* (Cambridge University Press, Cambridge, 2005).
- [3] Y. R. Shimizu, J. D. Garrett, R. A. Broglia, M. Gallardo, and E. Vigezzi, *Rev. Mod. Phys.* **61**, 131 (1989).
- [4] D. J. Dean and M. Hjorth-Jensen, *Rev. Mod. Phys.* **75**, 607 (2003).
- [5] G. F. Bertsch and H. Esbensen, *Ann. Phys.* **209**, 327 (1991); H. Esbensen and G. F. Bertsch, *Nucl. Phys.* **A542**, 310 (1992).
- [6] K. Ikeda, *Nucl. Phys.* **A538**, 355c (1992).
- [7] M. V. Zhukov, B. V. Danilin, D. V. Fedorov, J. M. Bang, I. J. Thompson, and J. S. Vaagen, *Phys. Rep.* **231**, 151 (1993).
- [8] K. Hagino and H. Sagawa, *Phys. Rev. C* **72**, 044321 (2005).
- [9] K. Hagino, H. Sagawa, J. Carbonell, and P. Schuck, *Phys. Rev. Lett.* **99**, 022506 (2007).
- [10] Y. Kikuchi, K. Kato, T. Myo, M. Takashina, and K. Ikeda, *Phys. Rev. C* **81**, 044308 (2010).
- [11] T. Nakamura *et al.*, *Phys. Rev. Lett.* **96**, 252502 (2006).
- [12] P. Mueller *et al.*, *Phys. Rev. Lett.* **99**, 252501 (2007).
- [13] R. H. Ibarra, N. Austern, M. Vallieres, and D. H. Feng, *Nucl. Phys.* **A288**, 397 (1977).
- [14] F. A. Janouch and R. J. Liotta, *Phys. Rev. C* **27**, 896 (1983).
- [15] F. Catara, A. Insolia, E. Maglione, and A. Vitturi, *Phys. Rev. C* **29**, 1091 (1984).
- [16] L. Ferreira, R. Liotta, C. H. Dasso, R. A. Broglia, and A. Winther, *Nucl. Phys.* **A426**, 276 (1984).
- [17] M. Matsuo, K. Mizuyama, and Y. Serizawa, *Phys. Rev. C* **71**, 064326 (2005).
- [18] N. Pillet, N. Sandulescu, and P. Schuck, *Phys. Rev. C* **76**, 024310 (2007).
- [19] N. Pillet, N. Sandulescu, P. Schuck, and J. -F. Berger, *Phys. Rev. C* **81**, 034307 (2010).
- [20] A. J. Leggett, in *Modern Trends in the Theory of Condensed Matter* (Lecture Note in Physics vol 115), edited by A. Pekalski and R. Przystawa, (Berlin Springer-Verlag, 1980).
- [21] A. J. Leggett, *J. de Phys.* **41**, C7-19 (1980).
- [22] P. Nozières and S. Schmitt-Rink, *J. Low Temp. Phys.* **59**, 195 (1985).
- [23] M. Matsuo, *Phys. Rev. C* **73**, 044309 (2006).
- [24] J. Margueron, H. Sagawa, and K. Hagino, *Phys. Rev. C* **77**, 054309 (2008).
- [25] T. Abe and R. Seki, *Phys. Rev. C* **79**, 054002 (2009).
- [26] S. S. Pankratov, E. E. Saperstein, M. V. Zverev, M. Baldo, and U. Lombardo, *Phys. Rev. C* **79**, 024309 (2009).
- [27] Y. Kanada-En'yo, N. Hinohara, T. Suhara, and P. Schuck, *Phys. Rev. C* **79**, 054305 (2009).
- [28] A. Pastore, F. Barranco, R. A. Broglia and E. Vigezzi, *Phys. Rev. C* **78**, 024315 (2008).
- [29] S. Yoshida, *Nucl. Phys.* **33**, 685 (1962).
- [30] D. R. Bes and R. A. Broglia, *Nucl. Phys.* **80**, 289 (1966).
- [31] R. A. Broglia, O. Hansen, and C. Riedel, "Two-Neutron Transfer Reactions and the Pairing Model" in *Advances in Nuclear Physics* vol.6, (Plenum, New York, 1973) ed. by M. Baranger and E. Vogt, pp.287-457.
- [32] A. Chatterjee *et al.*, *Phys. Rev. Lett.* **101**, 032701 (2008).
- [33] I. Tanihata *et al.*, *Phys. Rev. Lett.* **100**, 192502 (2008).
- [34] N. Keeley *et al.*, *Phys. Lett.* **B646**, 222 (2007).
- [35] M. S. Golovkov *et al.*, *Phys. Lett.* **B672**, 22 (2009).
- [36] J. Dobaczewski, W. Nazarewicz, T. R. Werner, J. F. Berger, C. R. Chinn, and J. Dechargé, *Phys. Rev. C* **53**, 2809 (1996).
- [37] E. Khan, N. Sandulescu, N. Van Giai, and M. Grasso, *Phys. Rev. C* **69**, 014314 (2004).
- [38] B. Avez, C. Simenel, and Ph. Chomaz, *Phys. Rev. C* **78**, 044318 (2008).
- [39] E. Khan, M. Grasso, and J. Margueron, *Phys. Rev. C* **80**, 044328 (2009).
- [40] D. R. Bes and R. A. Broglia, *Phys. Rev. C* **3**, 2349 (1971).
- [41] R. A. Broglia, D. R. Bes, and B. S. Nilsson, *Phys. Lett.* **B50**, 213 (1974).
- [42] H. J. Ong *et al.*, *Phys. Rev. C* **73**, 024610 (2006).
- [43] H. J. Ong *et al.*, *Phys. Rev. C* **78**, 014308 (2008).
- [44] Z. Elekes *et al.*, *Phys. Rev. C* **79**, 011302 (2009).
- [45] J. K. Jewell *et al.*, *Phys. Lett.* **B454**, 181 (1999).
- [46] E. Khan *et al.*, *Phys. Lett.* **B490**, 45 (2000).
- [47] N. Iwasa *et al.*, *Phys. Rev. C* **78**, 024306 (2008).
- [48] Y. Serizawa and M. Matsuo, *Prog. Theor. Phys.* **121**, 97 (2009).
- [49] M. Matsuo, Y. Serizawa, and K. Mizuyama, *Nucl. Phys.* **A788**, 307c (2007).
- [50] N. Paar, D. Vretenar, E. Khan, and G. Colo, *Rep. Prog. Phys.* **70**, 691 (2007).
- [51] M. Igarashi, K.-I. Kubo, and K. Yagi, *Phys. Rep.* **199**, 1 (1991).
- [52] W. von Oertzen and A. Vitturi, *Rep. Prog. Phys.* **64**, 1247 (2001).
- [53] G. Potel, B. F. Bayman, F. Bracco, E. Vigezzi, and R. A. Broglia, arXiv:0906.4298.
- [54] M. Matsuo, *Nucl. Phys. A* **696**, 371 (2001); *Prog. Theor. Phys. Suppl.* **146**, 110 (2002).
- [55] M. Bender, P.-H. Heenen and P.-G. Reinhard, *Rev. Mod. Phys.* **75**, 121 (2003).
- [56] E. Chabanat, P. Bonche, P. Haensel, J. Meyer, and R. Schaeffer, *Nucl. Phys.* **A635**, 231 (1998); *Nucl. Phys. A* **643**, 441 (1998).
- [57] E. Garrido, P. Sarriguren, E. Moya de Guerra, and

- P. Schuck, Phys. Rev. C **60**, 064312 (1999).
- [58] E. Garrido, P. Sarriguren, E. Moya de Guerra, U. Lombardo, P. Schuck, and H. J. Schulze, Phys. Rev. C **63**, 037304 (2001).
- [59] R. R. Chasman, Phys. Rev. C **14**, 1935 (1976).
- [60] J. Dobaczewski, W. Nazarewicz, and P.-G. Reinhard, Nucl. Phys. **A693**, 361 (2001).
- [61] J. Dobaczewski and W. Nazarewicz, Prog. Theor. Phys. Suppl. **146**, 70 (2002).
- [62] J. Dobaczewski, W. Nazarewicz, and M. V. Stoitsov, Euro. Phys. J. **A15**, 21 (2002).
- [63] M. Yamagami, Phys. Rev. C **72**, 064308 (2005).
- [64] M. Yamagami, Y. R. Shimizu, and T. Nakatsukasa, Phys. Rev. C **80**, 064301 (2009).
- [65] W. Satula, J. Dobaczewski, and W. Nazarewicz, Phys. Rev. Lett. **81**, 3599 (1998).
- [66] A. H. Wapstra, G. Audi, and C. Thibault, Nucl. Phys. **A729**, 129 (2003).
- [67] J. Terasaki, H. Flocard, P.-H. Heenen, and P. Bonche, Nucl. Phys. **A621**, 706 (1997).
- [68] J. Terasaki and J. Engel, Phys. Rev. C **74**, 044301 (2006).
- [69] A. Ansari and P. Ring, Phys. Rev. C **74**, 054313 (2006).
- [70] A. P. Severyukhin, V. V. Voronov, and N. Van Giai, Phys. Rev. C **77**, 024322 (2008).
- [71] A. P. Severyukhin, V. V. Voronov, and N. Van Giai, Eur. Phys. J. A **22**, 397 (2004).
- [72] S. Raman, C. W. Nestor, and P. Tikkanen At. Data Nucl. Data Tables **78**, 1 (2001).
- [73] D. C. Radford *et al.*, Nucl. Phys. **A752**, 264c (2005).
- [74] A. Banu *et al.*, Phys. Rev. C **72**, 061305 (2005).
- [75] C. Vaman *et al.*, Phys. Rev. Lett. **99**, 162501 (2007).
- [76] J. Cederkäll *et al.*, Phys. Rev. Lett. **98**, 172501 (2007).
- [77] A. Ekström *et al.*, Phys. Rev. Lett. **101**, 012502 (2008).
- [78] M. A. Kennedy, P. D. Cottle, and K. W. Kemper, Phys. Rev. C **46**, 1811 (1992).